Improving the performances of direct-current triboelectric nanogenerators with surface chemistry

Xin Lyu[a], Simone Ciampi[a,*]

[a]School of Molecular and Life Sciences, Curtin University, Bentley 6102 Western Australia, Australia
*Correspondence: simone.ciampi@curtin.edu.au

Abstract

Over the past decade, triboelectric nanogenerators (TENGs) – small and portable devices designed to harvest electricity from mechanical vibrations and friction – have matured from a niche theme of electrical engineering research into multidisciplinary research encompassing materials science, physics and chemistry. Recent advances in both the fundamental understanding and performances of TENGs have been made possible by surface chemistry, electrochemistry and theoretical chemistry research entering this active and promising field. This short review focuses on the recent developments of direct-current (DC) TENGs, where sliding friction or repetitive contact–separation cycles between the surface of polymers, metals, chemically modified semiconductors, and more recently even by the simple contact of surfaces with water solutions, can output DC suitable to power electronic devices without the need of additional rectification. We critically analyze the role of surface chemistry towards maximizing DC TENG outputs and device longevity. The major current hypotheses about their working mechanism(s) are also discussed.

Keywords

Triboelectric nanogenerators; Schottky diodes; static electricity; flexoelectricity; surface chemistry; organic monolayers

Introduction

Portable technologies that in the last three decades have reshaped our social, economic, and cultural environments rely on electronics that are powered by DC current. There is therefore an ever increasing demand for small, portable, regenerative and autonomous DC energy sources [1]. Most electronics still rely on non-regenerative power sources – commonly batteries – which have limitations such as a limited lifespan [2, 3]. Furthermore, the growing popularity

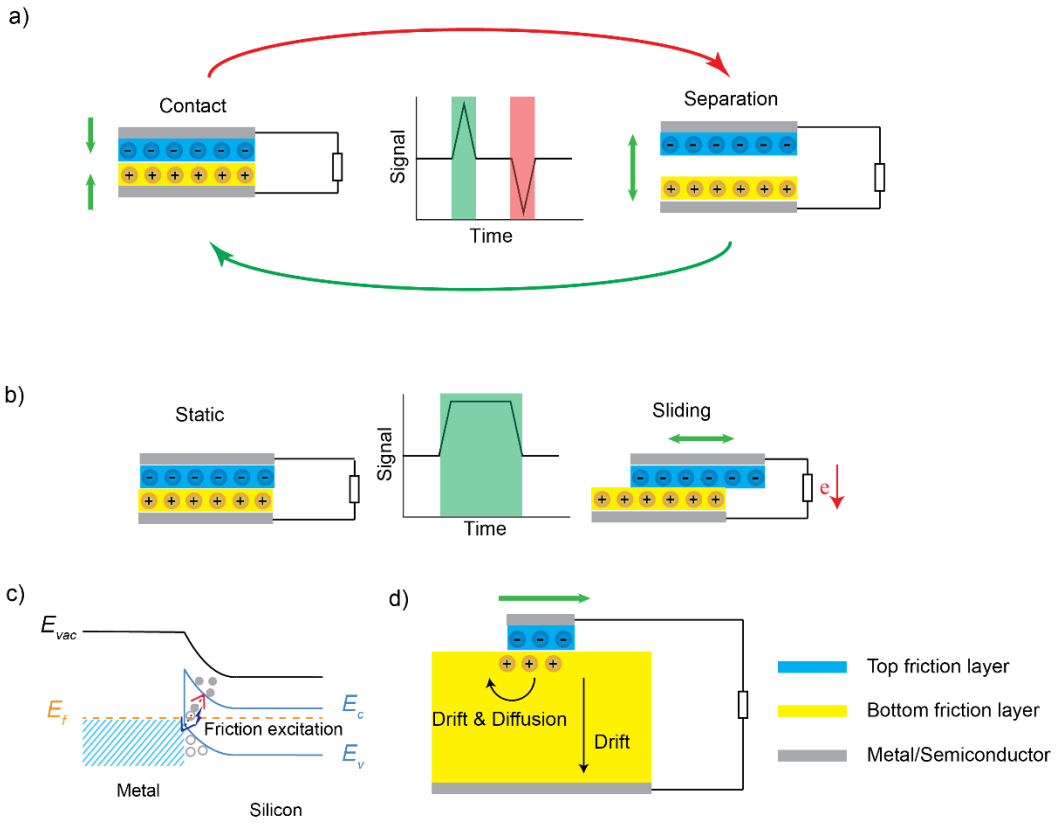

Figure 1. (a) Schematics of the contact–separation mode of AC TENGs. The inset shows the AC signal recorded during a cycle of contact and separation. (b–c) Schematics of the tribovoltaic/flexoelectric effect [8, 9] behind the operation of semiconductor-based sliding mode DC TENGs. (d) Depiction of the dynamic formation and equilibration of a space-charge layer leading to a competition between drift and diffusion. The sign of the charges as well as the current flow direction depends on surface characteristics, such as work function, ionization energy, electron affinity, and presence/absence of electronic defects.

of wearable and implantable devices has created a need for smaller, and ideally biocompatible, power units [4-7]. Thus, autonomous, regenerative, microscale or even nanoscale, biocompatible energy source technologies are in growing demand.

Triboelectric nanogenerators (TENGs) are a promising source of sustainable and autonomous electricity, whose purpose is that of converting ubiquitous mechanical vibration/friction, such as thermal vibrations [10, 11], muscle movements [12], ultrasonic or ocean waves [13-15] into either AC or DC, and which open up to energy, sensing, and medical applications [16-18]. Their working modes can be tentatively grouped into four main categories: contact–separation, sliding, lateral single-electrode, and freestanding triboelectric-layer [19-23]. The creation of a potential difference between top and bottom electrodes in relative motion, is generally electrostatic in nature. TENGs' common designs, as shown in Figure 1, include a top and a bottom friction layer, usually made of metals [24], semiconductors [25], organic polymers [26], 2D materials [27], or even water [28]. The contact–separation mode (Figure 1a) is most

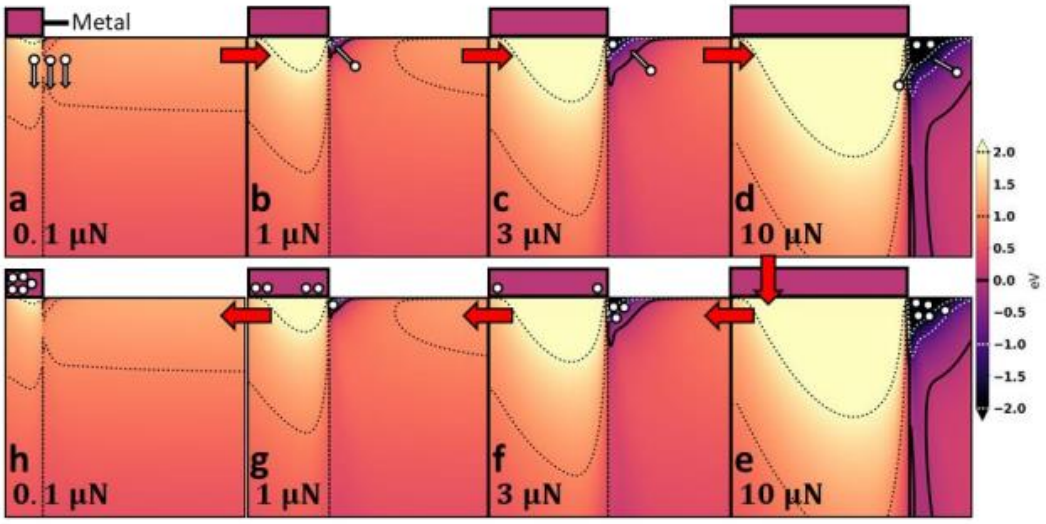

Figure 2. Band bending and ratcheting mechanism for metal (purple block) –semiconductor (orange block) contacts under a cyclic change in pressure. (a–d) While the force applied is ramped, electrons (illustrated by white circles) accumulate on the semiconductor side of the junction. (e–g) When the load is removed, the number of available states for electrons in the potential well drops, forcing some electrons to migrate into the metal. (h) The electrons have mostly been transfer into the metal after the external force is completely released. Adapted from the study by Olson et al. [8], copyright (2022), with permission from American Chemical Society.

common among AC TENGs, where the top and bottom friction layers are usually electrically insulating organic polymers such as polyethylene terephthalate (PET) or polytetrafluoroethylene (PTFE) [20, 29]. Here surface charging is mainly due to static electrification, which builds up in part after the transfer of charged molecular fragments (vide infra). Electrons will move in the external circuit to balance the polymer charges, and upon separation of the two dielectrics current will flow to bring the system back to equilibrium. In essence, an AC current flows in the external circuit with the same frequency of the contact–separation events. For DC TENGs, the sliding mode is generally more prevalent (Figure 1b,c) with often one of the electrodes being a semiconductor.

The actual TENGs mode(s) of action if still debated, with some authors arguing in favor of discharge of static electricity being the major driving force [1, 30, 31], others invoking an imbalance between migration and diffusion of surface charges (Figure 1d) [32], and some arguing for a unidirectional movement of friction- or pressure-induced electron–hole pairs – the tribovoltaic effect – being the main mechanism (Figure 1c) [33-37]. In addition, and probably contributing to the first and latter mechanisms, there is flexoelectricity (Figure 2): a band bending and ratcheting mechanism where subsequent compression/decompression of the metal–semiconductor junction forces electrons to move preferentially in one direction [8, 9].

Mechanistic studies on the ratcheting mechanism were conducted on highly doped semiconductor materials [8], but it is not clear if this will still be valid for dynamic junctions made on lowly-doped semiconductor materials where, among other factors, the space charge region is much thicker. For instance, unlike the recent finding of Marks and co-workers [8], most silicon-based TENGs yield tribocurrents with the direction of a leakage current, indicating that the interfacial field formed upon contact moves electrons either via avalanche breakdown or tunneling. Which of the two dominates is still unclear, and answering this question will probably require designing experiments where the temperature of the sliding junction can be either controlled or at least monitored.

The debate on to what extent contact electrification is key to the operation of TENGs will not be resolved until a consensus is reached on the nature and origin of statics [32, 38, 39]. A small digression on triboelectricity is therefore needed here, first to explain why objects that cannot conduct electricity become charged in the first place. The term electron comes from the Greek word for amber – "elektra", later Latinised in "electra" – and Thales of Miletus, who lived around the 600 B.C., left accounts of the ancient Greeks being aware of chicken's feathers being attracted to amber after its contact with rabbit's fur. The most striking properties of electrified object is in fact that of attraction and repulsion, but it was not until the 17th century that materials other than amber, such as glass and sulphur, were also found to gain a static charge after contact and separation. The topic remained a scientific curiosity until the 18th and 19th centuries, when polymaths like Benjamin Franklin and Michael Faraday initiated its systematic study. It finally gained the attention of engineers and chemists in the 1970s, when the development of copiers and laser printers created a strong incentive to understand the chemistry behind the triboelectrification of plastic polymers [40]. A common misconception is that electrification upon contact is limited to plastic polymers, but just as the demarcation between insulators and conductors is arbitrary, so it's a material ability to statically charge. Metals and semiconductors exchange charges upon contact [41], but because charges are here free to move, the result is that it becomes harder to accumulate them so to reach large voltages, noting that surface voltages in the excess of 30 kV/cm can be easily obtained on insulators. The nature of this charge is still debated. Do free electrons move upon contact [42, 43], are ionic species formed upon the mechanical breaking of bonds asymmetrically transferred [44], is there a role played by redox chemistry of reactive functional groups [45, 46], or is statics mainly the transfer of water-derived ions [47-51]? A lot of this is still not clear [39, 52-54]. Moreover, non-polar plastics such as PTFE and polyethylene becomes very charged, which is

hard to expected based on their chemistry, and several materials form a cyclic, instead than linear, triboelectric series, suggesting that the triboelectrification process does not simply rely on a single physical characteristic [54, 55]. The shape of the object is also important [56], as well as its softness [57, 58]. What is clear beyond ambiguity is that statics is dominated by surface rather than bulk material properties. Interestingly this aspect was already appreciated in the 19th century, when it became apparent that the position of metals in the Volta series depended on whether measurements were done in air or under hydrogen sulfide, with for example copper and iron swapping position in the series in response to this.

The application of several areas of chemistry, most importantly of surface chemistry and electrochemistry, towards answering the question as to what are the charge-carrying species [56, 58, 59] is assisting today the development of TENGs as it did in the 1970s during the development of xerography [60, 61]. The scope of this short review is therefore to summarize the scope of surface chemistry towards maximizing the performances of DC TENGs, as well as its contribution in unveiling the actual energy conversion mechanism of TENGs.

As shown in Figure 1a, the dielectric-displacement current generated by traditional (polymer-based) TENGs, such as in the sliding-mode design is AC. Besides the requirement of rectification in order to power up microelectronic devices, the impedance of polymers is a crucial constraint to the achievable current density. Both issues are removed in metal–semiconductor (Schottky diodes) TENGs [62, 63]. Semiconductors such as silicon are used in DC TENGs owing largely to the versatility of its surface chemistry [64-66], low costs [67], and an high output current density – over 10^9 A/m^2 in micro/nanoscale [68] and up to 200 A/m^2 in macroscale [69]. Furthermore, by tethering organic monolayers it is possible to tune the interface charge transport characteristics, adhesion, and friction [52, 66, 70-73]. As briefly mentioned above, omitting the nuances of flexoelectricity, the main mechanism is here a tribovoltaic effect [33-37], which in first approximation is analogous to the photovoltaic effect, and is schematically depicted in Figure 3 for a sliding p–n junction [25] but will also be applicable to metal–semiconductor Schottky diodes [35]. The current generation process involves tunneling (or avalanche breakdown) across the metal–insulator–semiconductor structure [74, 75]. Electron–hole pairs excited by friction are separated by the built-in electric field at the interface, hence the current flows in the same direction of the leakage current. Indeed the surface chemistry is quite crucial here, as it is capable of engineering surface properties such as work function, electric field, and charge transfer, to eventually tune the leakage [76, 77].

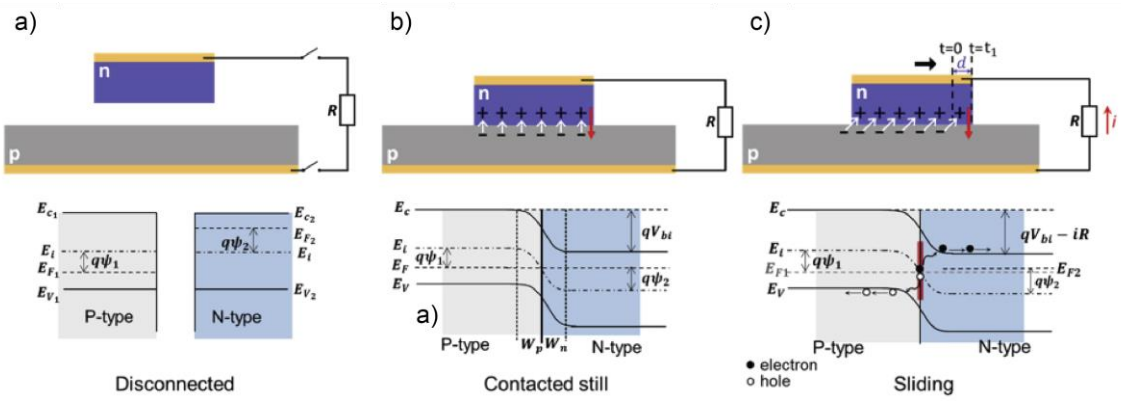

Figure 3. Schematics and energy band diagrams for a DC TENG by using a n-type semiconductor as top electrode sliding on the surface of a p-type semiconductor (bottom electrode). Illustration of the condition of (a) disconnected, (b) contacted still, and (c) lateral sliding of the p–n junction. The white arrows represent the surface dipole moment, and the red arrows represent the direction of the built-in electric field. E_C is the bottom of the conduction band, E_V is the top of the valence band, E_i is the intrinsic level of the pure semiconductor without doping and E_F is the Fermi level, V_{bi} is the built-in electric field potential, $\psi_{1,2}$ are the potentials with respect to the Fermi levels in the p- and n-type semiconductors. Adapted from the study by Xu et al. [25], copyright (2019), with permission from Elsevier.

But for such silicon-based DC TENGs the substrate is an non-oxide semiconductor prone to oxidation, a reaction that will inevitably cause drops in surface conductivity and open-circuit voltages (V_{oc}) [75]. Although some extent of oxidation can introduce surface states that counterintuitively increase conductivity [78], this effect is only transient. The oxide layer (silica) can be removed via chemical etching, but eventually the etched surface (Si–H) [79-81] oxidizes again after exposure to the environment [82, 83]. To limit this, several surface modification strategies involving organic and inorganic chemicals, as well as metals, have been proven viable [73, 84-87]. In the following, we present surface modification strategies for TENG materials and discuss their pros and cons.

Surface modification of triboelectric materials

Organic materials

Organic molecules that can self-assemble on metals and semiconductors are a first choice in terms of improving the performances of a TENG. In 2006 Akbulut and co-workers [24] coated Au, Ag and Ti surfaces with self-assembled monolayers (SAMs) of 1-hexadecanethiol so to prevent these metals from cold-welding, a phenomenon that inhibits the relative movement of metals and leads to material wear [88]. Interestingly the authors observed large current fluctuations when sliding different (SAM-passivated) metals against each other, while no charge transfer was observed when identical metals were sheared. For SAMs-coated Ag and Au surfaces the authors observed DC current densities up ~20 mA/m^2. The authors suggest a

continuous entangling and disentangling, and cyclic deformation and relaxation, of SAM chains during sliding. They also speculate that amorphous SAM regions may be capable of assisting charge transport even under static conditions. These two effects, may contribute to the triboelectrification of the contact. According to the authors, the lag between current and friction after having stopped the sliding could be evidence of a slow SAM relaxation. Further studies will need to be conducted to prove a relationship between monolayer order and propensity to gain static charges. Further, as only one type of SAM was explored, an open question remains, that is whether or not different SAMs, for instance with different polarity and wettability, will show a similar delay.

Similarly, in 2016 Wang and co-authors [89] used Au substrates functionalized with thiol-based SAMs as materials for AC contact–separation TENGs. They investigated five SAMs with either hydroxyl (–OH), methyl esters (–C(O)OCH_3), amines (–NH_2), aniline (–C_6H_5–NH_2), or chloro (–Cl) functionalities as terminal group. These SAMs were formed onto an Au film deposited on Kapton by e-beam evaporation, and with a 100 nm copper layer deposited on fluorinated ethylene propylene (FEP) film (vapor deposition) as the second electrode. Under mechanical shaking (~2.5 Hz), –NH_2 surfaces showed the greater surface potential by Kelvin probe force microscopy (KPFM), and were the most effective nanogenerator, with the charge density reaching ~140 μC/m^2, and the open-circuit voltage (V_{oc}) and short-circuit current density (J_{sc}) reaching ~560 V and ~18.5 mA/m^2, respectively. For almost all the surface chemistries investigated, TENG performances were significantly higher compared to controls with unmodified surfaces. The only exception were chloro-terminated surfaces. Furthermore, the same authors also explored amine-terminated silane-based SAMs grafted on SiO_2 surfaces. The charge density, V_{oc}, and J_{sc} increased from ~34 μC/m^2, ~150 V and ~0.7 mA/m^2 (respectively) on the SiO_2 surface, to ~51 μC/m^2, ~240 V, and ~1.75 mA/m^2 for the modified systems. Although the output of these TENGs is AC, these results indicate a scope for the improvement of DC TENGs by surface chemistry, focusing especially on the material electronegativity. The authors recommended head groups with lower electronegativity for the positive side, higher electronegativity for the negative side, and longer chains.

Inspired by the research discussed above, Ciampi and co-workers [84] investigated covalent 1,8-nonadiyne monolayers (Si–C-bound) grafted on NH_4F-etched 111- and 100-oriented silicon substrates (**S1**, Figure 4a). The monolayer purpose is first to prevent substrate oxidation, and second to engineer charge transport on Si(111) pyramids etched on a Si(100) surface. Using platinum AFM tips as the sliding metal contact it is possible to measure simultaneously surface

properties (such as friction and topography) as well as the zero-bias current. The topography (Figure 4b) as well as the leakage current (under an external bias) and zero-bias (TUNA) current signal along the red dotted line (Figures 4b,c) were recorded simultaneously. The maximum DC current density for such structure was of 2.9×10^5 A/m^2. Interestingly, the recorded zero-bias current reaches a peak at concave boundaries between the (100) and (111) planes, rather than at the convex pyramid [Si(100)] apex. The tribocurrent, which bears the sign of a reverse-bias current, interestingly also does not track the leakage current of static junctions (estimated from current–voltage characteristics, Figure 4c). The authors suggest that the Schottky barrier may be decreasing under increasing stress, and that the concave curvature at the pyramid's base leads to a thinner space charge. Using a semiconductor as readily available as silicon could significantly reduce the costs of DC TENGs, as well as ensure compatibility with mainstream electronics, but such textured surface (pyramids) introduce some level of complexity in the preparation of such devices. Thus, exploring flat and unstructured silicon, and the influence of surface chemistry on performance of Schottky diode-based DC TENGs (Figure 4a, **S2-X**, with X being either $–NH_2$, –OH or $–CH_3$ groups), Ferrie et al. modified Si(111) crystals by Cu-catalyzed azide–alkyne cycloaddition (CuAAC) reactions [73]. Polar groups ($–NH_2$ and –OH) led to a greater zero-bias DC current output, which parallels the findings for AC TENGs by Wang et al. discussed above [89]. It is therefore possible to augment DC current output on flat silicon by means of surface functionalization, even though the two-step (passivation followed by functionalization) procedure involved is laborious. In an attempt to simplify the surface chemistry aspects, Lyu et al. attempted to use 1,8-nonadiyne, 1-nonyne, 1-nonanol, and 8-nonyn-1-ol to form in one step alkynyl (–C≡CH), alkyl ($–CH_3$), and hydroxyl (–OH) monolayers, as shown in Figure 4d [68]. With platinum as the sliding metal contact, 8-nonyn-1-ol coated Si(211) showed a maximum current density of ~10^9 A/m^2. One of the most important factors causing hydroxyl-terminated Si(211) surfaces to perform well is surface polarity coupled to a relatively large surface recombination and velocity, plus the negative charge on the metal tip owing to flexoelectricity [68].

Polymers have also continued to gain popularity as triboelectric material for DC TENGs. Recently You et al. [90] have successfully coated poly-3,4-ethylene dioxythiophene:poly-styrene sulfonate (PEDOT:PSS) on aluminum alloy films as top friction layer, and used Al alloys, Si, ITO, Cu, and graphene as bottom friction layer in sliding mode TENGs, as shown

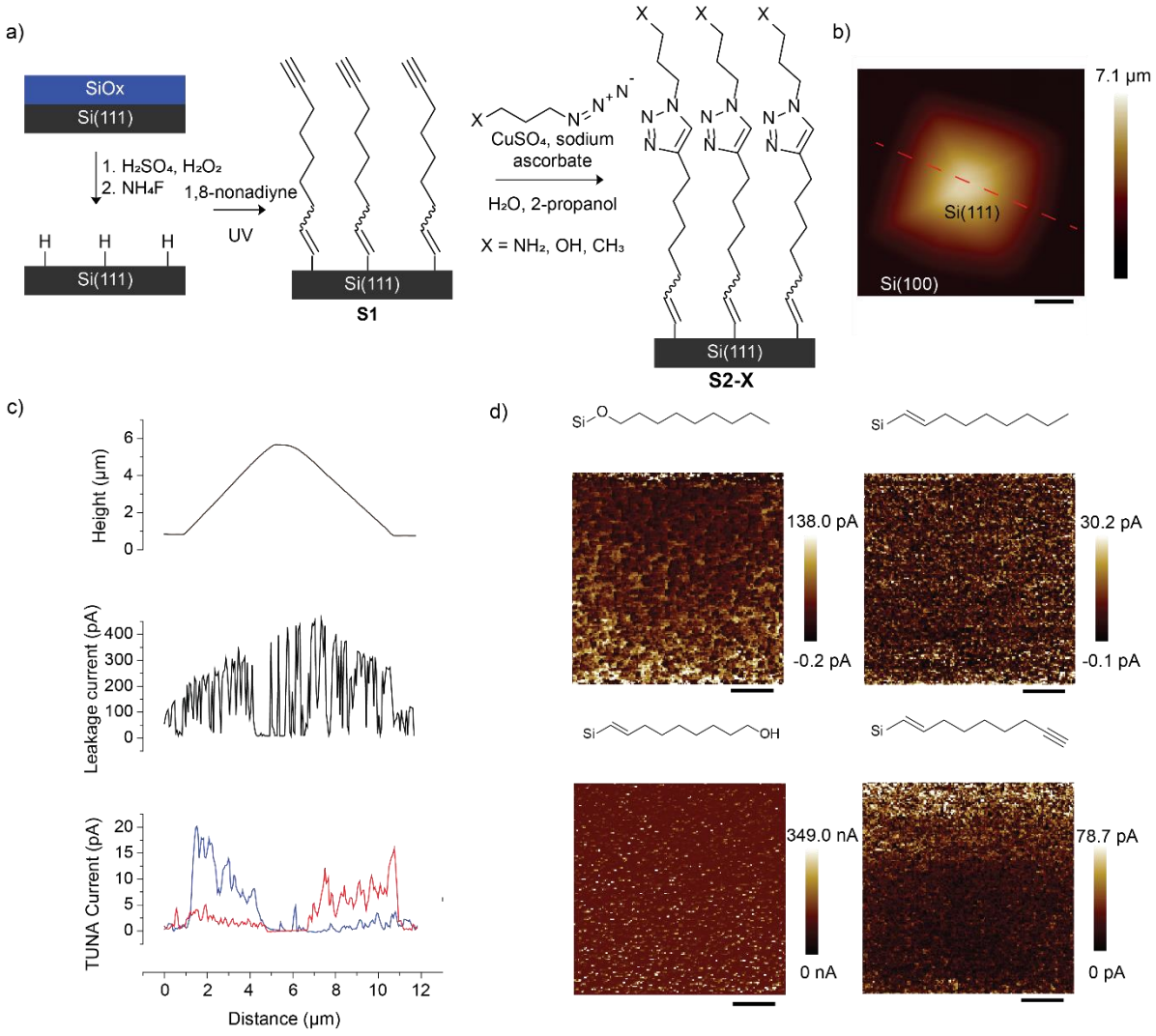

Figure 4. (a) Oxide-free silicon surface functionalization. Native oxide is first cleaned and etched (steps 1 and 2) to form a hydrogen-terminated surface. This surface is reacted under UV with 1,8-nonadiyne to form surface **S1**. The terminal alkyne functionality of **S1** is reacted through a CuAAC reaction to covalently attach either 3-azidopropan-1-amine (forming **S2-NH$_2$**), 3-azidopropan-1-ol (**S2-OH**), or 1-azidobutane (**S2-CH$_3$**). Adapted from the study by Ferrie et al. [73], copyright (2022), with permission from Elsevier. (b) 12 × 12 µm AFM height image of Si(111) pyramids on lowly doped float zone (FZ) n-type Si(100). (c) Topography, leakage current (under an external bias), and zero-bias tunneling AFM (TUNA) current profiles over the dotted red line in (b). Trace data are in blue, and retrace data in red. Adapted from the study by Ferrie et al. [84], copyright (2022), with permission from Elsevier. (d) Zero-bias C-AFM 5 × 5 µm current maps of dynamic sliding Pt–Si(211) diodes. Oxide-free Si(211) samples were coated with monolayers of 1-nonanol, 1-nonyne, 8-nonyn-1-ol, and 1,8-nonadiyne. Adapted from the study by Lyu et al. [68], copyright (2022), with permission from Elsevier.

in Figure 5a. They conclude that the work function of the triboelectric material is the main factor influencing the DC TENGs output, as the work function difference correlates to the open- circuit voltage. As shown in Figure 5b, they also found out that the PEDOT:PSS/Al alloy device exhibits the greatest performance with a V_{oc} of 1 V, a I_{sc} of 309 µA, and power density

of 11.67 mW/m^2. After 1,000 successive bending events there is a reduction in the device open-circuit voltage, which highlights general concerns about the durability of TENGs. The decay of electrical performances is mainly due to frictional wear, which is the primary failure factor in TENGs [91-93].

Physical methods can also be applied to improve the output of DC TENGs. As shown in Figure 5c, Chen et al. [94] added a pre-charged PTFE layer that was charged by 100 cycles of manual rubbing against nitrile rubber, also known as field enhancing layer (FEL). This layer is placed under the triboelectric layer (PTFE), then the copper tape attaching to the acrylic sheet was slid against the triboelectric layer to generate DC current under different acceleration (contact area of 2 × 2 cm). A current of ~200 nA and an open-circuit of ~50 V were recorded. To scale this up, the authors also designed a rotary mode TENG using the same materials to realize a constant DC current output which can power a LED array without intermitted flashing.

Inorganic materials

Various inorganic materials have been utilized to modify the surface of TENGs and improve their performances and durability. In 2007, Wang and co-workers [13] used ZnO nanowires (bottom electrode) and a surface-engineered silicon jagged electrode coated with Pt (top electrode) to develop a nanogenerator able to harvest DC electricity from ultrasonic waves. This zigzag-shaped silicon electrode can effectively enlarge its surface area, favouring contact with the nanowires. Under ultrasonic waves, the nanowires continuously act like brushes on the silicon electrode. Analogously, Xu et al. [25] used HF-etched phosphorus-doped and boron-doped silicon as sliding electrodes, with an Au coating on both electrodes as a back contact as illustrated in Figure 5d. They managed to continuously harvest ~50 nA of DC current under 1 N of load (Figure 5e), and found that the current direction matches the built-in electric field of the junction. The authors also performed experiments under variable sliding speed, acceleration and length of the top electrode. They observed a positive correlation between the short-circuit current and these three parameters. This design indeed provides a high current output and supports a relationship between current, velocity and acceleration. The long-term performances of such structure is likely not to be outstanding as the silicon electrodes were only etched with HF solutions and no protective layer was incorporated in the design. The above mentioned issue of substrate re-oxidation and frictional wear remains a challenge, and to specifically address this, in 2018 Lin et al. [27] attempted to harvest DC by sliding graphene layers on silicon substrates (Figure 5f), given that graphene is self-lubricant. The authors reported DC

current densities up to 40 A/m^2, and stable outputs even after 10,000 cycles. Similarly, in 2021 Huang et al. [32] used Au coated highly ordered pyrolytic graphite, prepared via electron beam lithography, electron beam evaporation, and reactive ion etching, as the top electrode, and etched n-type silicon as the bottom electrode. They fabricated a superlubric Schottky based generator (Figure 5g) with current and power density of ~210 A/m^2 and ~7 W/m^2 respectively. Such device is also capable of maintaining such high performances for over 5,000 cycles. Notably, the authors exclude a friction-induced excitation mechanism and propose a mechanism based on the continuous establishment and destruction of the depletion layer. In simple terms, the net current flow is attributed to the electronic drift induced by non-equilibrium electric field over the movement between the triboelectric materials, as shown in Figure 5h. Such friction-less (or minimal friction) approach defines another direction for the future improvement of outputs and durability of DC TENGs.

The two designs outlined above rely on carbon-based materials (graphite or graphene) owing to their capacity of reducing friction [95]. Such designs undoubtedly reduce device wear, but the other contact material (silicon) was somehow neglected and in fact only treated with HF or buffered oxide etch solution to remove the native oxide. Obviously, etched silicon will re-oxidize in ambient air [79, 96] and due to a growing oxide layer current outputs will drop significantly and rapidly [75]. It is therefore surprising that this degradation was not observed as the electric field should further speed up the oxidation process [97, 98].

Protection of silicon against anodic decomposition is therefore imperative. Lu et al [99] attempted to coat HF-etched silicon substrates with AlN, HfO_2, or Al_2O_3 via physical vapor and atomic layer deposition. As shown in Figure 5i, using black phosphorus flakes, whose intrinsic anisotropy produces outstanding electronic, transport and mechanical characteristics [100], as the other triboelectric material, they built a Schottky diode sliding DC TENG and recorded an open-circuit voltage of 6.1 V and a short-circuit current density of 124.0 A/m^2 (power density of 201.0 W/m^2) for black phosphorus/AlN/Si heterojunction system. In 2020, they attempted to fabricate DC TENG using HF-etched and oxide-free n–n silicon homojunction, recording a current density of 214 A/m^2 and a voltage of 0.35 V [101]. They further explored the influence of different insulated dielectric layers (ZnO, HfO_2, Al_2O_3) on the performance of the silicon–dielectric layer–silicon system, and found out that the n-type Si/Al_2O_3/ n-type silicon can enhance the output voltage to 1.3 V.

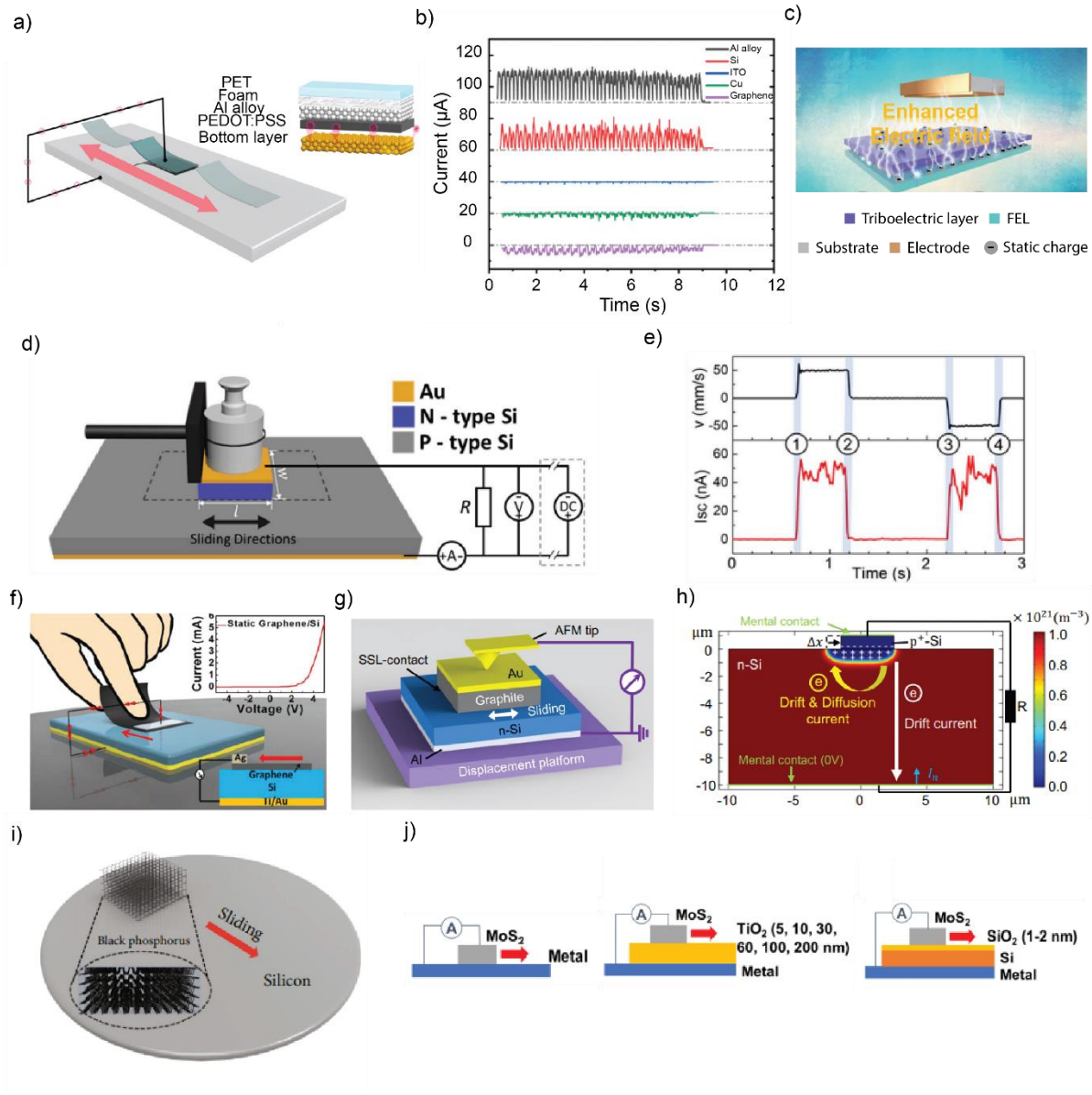

Figure 5. (a) Schematic of a DC TENG where changes to the bottom friction layer (an Al alloy, Si, ITO, Cu, or graphene) are reflected in drastic changes to the short-circuit current (b). Adapted from the study by You et al. [90], copyright (2022), with permission from Elsevier. (c) Schematic of a DC TENG where pre-charged PTFE, used as field-enhancing layer (FEL), is embedded under the triboelectric layer (PTFE). Adapted from the study by Chen et al. [94], copyright (2021), with permission from Wiley-VCH GmbH. (d) Schematic and external circuit of a p–n junction based TENG. (e) Sliding velocity and corresponding short-circuit current during the reciprocating movement of the slider shown in (d). Adapted from the study by Xu et al. [25], copyright (2019), with permission from Elsevier. (f) Experimental set-up for a sliding graphene–silicon TENG. The inset is an I–V curve of the static graphene–silicon junction. Adapted from the study by Lin et al. [27], copyright (2019), with permission from Wiley-VCH GmbH. (g) Experimental set-up for sliding superlubric graphite coated Ag-silicon Schottky diode triboelectric nanogenerator. (h) Simulation mode structure and the proposed physical process of the depletion layer establishment and destruction (DLED) mechanism. The scale bar on the right side represents the electron concentration. Adapted from the study by Huang et al. [32], copyright (2022), with permission from Nature Portfolio. (i) Schematic of the black phosphorus-coated Ag–silicon Schottky diode DC TENG. Adapted from the study by Lu et al. [99], copyright (2019), with permission from American Association for the Advancement of Science. (j) Schematic of a MoS_2–Si Schottky sliding diode DC TENGs in three

different structures (from left to right): metal–semiconductor (MS), metal–insulator–semiconductor (MIS), and semiconductor–insulator–semiconductor (SIS). Adapted from the study by Liu et al. [102], copyright (2019), with permission from American Chemical Society.

Afterwards, they intentionally used water as the dielectric material and moved it at the gap between HF etched n-type and p-type silicon. In response to the movement of water droplets, a DC voltage of 0.3 V and a current of 0.64 μA was recorded [103]. The authors proposed a new dynamic semiconductor–liquid–semiconductor structure DC TENG, which has the potential to obtain electricity from the motion of water, for instance from rain.

Analogous insulated dielectric materials between triboelectric materials are commonly used in the fabrication of DC TENGs. Liu et al [62] firstly attached a molybdenum disulfide (MoS_2) multilayer to the silver coated Si/SiO_2 substrates by pulsed laser deposition, and successfully harvested DC electricity from such structure with current density reaching up to 10^6 A/m^2. To further research on the enhancement of the MoS_2 based TENGs direct-current generation, the same authors attempted three different structures: metal–semiconductor (MS), metal–insulator–semiconductor (MIS), and semiconductor–insulator–semiconductor (SIS) (Figure 5j). The authors suggest that the DC output can be manipulated by interfacial engineering [102], and probed the influence of the insulator (SiO_x) thickness on the electrical performance of the sliding metal–insulator–semiconductor (Si) based DC TENG, and concluded that the short-circuit current slightly increases at the beginning and eventually decreases significantly with the increasing oxide layer thickness. And for native oxide with a thickness less than 2 nm on silicon substrates, the theoretical current density of such a metal-insulator-semiconductor system can reach up to 10^4 A/m^2 [75].

Sharov et al. [104] attached an InP layer, with its native oxide, on the HF-treated p-type Si(111), and use a silicon AFM tip with platinum or diamond coating as top contact. A peak and average current density in dark of 15 kA/m^2 and 7.3 kA/m^2 were reported. The authors also probed the photovoltaic efficiency in both the static and sliding regimes, reporting a 7% conversion efficiency. It provides a platform for coupling tribovoltaic and photovoltaic current generation.

Table 1. Surface functionalization and electrical performances of DC TENGs

Materials	Surface modification	Test cond.	I_{sc}	V_{oc}	J_{max} A/m^2	Ref
		Organic materials				
Ag [Au]	SAMs (1-hexadecanethiol)	Sliding			~0.02	[24]
Si(111) & Si(100) [Pt]	SAMs (1,8-nonadiyne)	Sliding			2.9×10^5	[84]
Si(111) [Pt]	SAMs & CuAAC ($–NH_2$, –OH, $–CH_3$)	Sliding			4.6×10^6	[73]
Si(211) [Pt]	SAMs ($–CH_3$, –OH, $–C\equiv CH$)	Sliding			4.9×10^9	[68]
PEDOT:PSS [Al]	poly-3,4-ethylene dioxythiophene: poly-styrene sulfonate	Sliding	309 µA	1 V		[90]
PTFE [Cu]	Pre-charged PTFE	Sliding	200 nA	50 V		[94]
		Inorganic materials				
ZnO nanowires [Si zigzag]		Ultrasonic Wace	0.15 nA			[13]
Si [graphene]	HF etched	Sliding			40.0	[27]
Si(100) [graphite]	Buffered oxide etch	Sliding			~210	[32]
p-type Si [n-type Si]	HF etched	Sliding	50 nA			[25]
Si [black phosphorus]	Deposition (AlN, HfO_2, Al_2O_3)	Sliding		6.1 V	124	[99]
n-type Si [n-type Si]	HF etched	Sliding		0.35 V	214	[101]
n- & p-type Si [water]	HF etched	Sliding	0.64 µA	0.3 V		[103]
Ag [Si tip]	Pulsed laser deposition (MoS_2)	Sliding			~10^6	[62]
p-type Si(111) [diamond coated Si tip]	Molecular beam epitaxy (InP)	Sliding		15 mV	1.5×10^4	[104]

Conclusions

Autonomous power supplies that converts mechanical energy into electricity take on a vital role when it is not possible to replace or recharge a battery, such as in life-critical medical implants or sensors in remote/dangerous places. The environment provides a broad range of mechanical energy sources, but in a nanoscale setting conversion of mechanical energy into direct current remains a challenge. By merging innovations in both surface science and electrical engineering, DC triboelectric nanogenerators (DC TENGs) are becoming a viable path to miniature power supplies. Surface chemistry and surface microfabrications protocols have been extremely valuable, and for example shown that engineering sharp lateral changes in the semiconductor barrier is dramatically more effective towards maximizing current than increasing the applied normal force, or the surface friction [84]. This is a path towards removing friction – and therefore area – constraints. It is also a path towards limiting device wear: tribocurrent densities can be enhanced under minimal friction. More recently zero-

applied-bias current densities as high as 10^9 A/m^2 have been achieved using a proton-exchangeable organic monolayer that simultaneously introduces a sufficiently high density of surface states (assessed as changes to carrier recombination velocities) coupled to a strong surface dipole in the form of a surface alkoxide anion (Si–monolayer–O^-) [68]. These are just key examples, and a more comphrensive summary of the status of DC TENGs systems is in Table 1. To futher improve the performance of DC TENGs, including their power density and durability more surface chemistry research is needed. Furthermore, the mechanism by which DC TENGs operate remains controversial. Among the key pending questions we believe the following are particularly pressing:

1. For DC TENGs that are essentially out-of-equilibrium diodes, the DC output grows or declines with the level of surface states?
2. Is it all governed by the movement of charged molecular fragments or by flexoelectricity?
3. Is stick–slip friction involved, or are pressure fluctuations more important than lateral friction?
4. Is surface water involved? Is the charge of the aerial surface of water playing a role? Or a wet interface is just leading to a larger contact?

Apart from these questions, we hope DC TENGs research will succeed in bringing surface scientists and electrochemists closer to a definitive understanding on the origin of static electricity, a puzzle that has been fascinating scientists and engineers since the antiquity.

Conflict of interest statement

The authors declare that they have no known competing financial interests or personal relationships that could have appeared to influence the work reported in this paper.

Acknowledgements

S.C. acknowledges support from the Australian Research Council (grant no. FT190100148).

References

Papers of particular interest, published within the period of review, have been highlighted as:

* of special interest

* * of outstanding interest

1. Wu, C.; Wang, A. C.; Ding, W.; Guo, H.; Wang, Z. L., **Triboelectric nanogenerator: A foundation of the energy for the new era.** Adv. Energy Mater. 2019, **9:**1802906. http://doi.org/10.1002/aenm.201802906

2. Niu, S.; Wang, Z. L., **Theoretical systems of triboelectric nanogenerators.** Nano Energy 2015, **14:**161–192. http://doi.org/10.1016/j.nanoen.2014.11.034

3. Salauddin, M.; Toyabur, R. M.; Maharjan, P.; Rasel, M. S.; Kim, J. W.; Cho, H.; Park, J. Y., **Miniaturized springless hybrid nanogenerator for powering portable and wearable electronic devices from human-body-induced vibration.** Nano Energy 2018, **51:**61–72. http://doi.org/10.1016/j.nanoen.2018.06.042

4. Zheng, Q.; Shi, B.; Li, Z.; Wang, Z. L., **Recent progress on piezoelectric and triboelectric energy harvesters in biomedical systems.** Adv. Sci. 2017, **4:**1700029. http://doi.org/10.1002/advs.201700029

5. Su, Y.; Wang, J.; Wang, B.; Yang, T.; Yang, B.; Xie, G.; Zhou, Y.; Zhang, S.; Tai, H.; Cai, Z.; Chen, G.; Jiang, Y.; Chen, L.-Q.; Chen, J., **Alveolus-inspired active membrane sensors for self-powered wearable chemical sensing and breath analysis.** ACS Nano. 2020, **14:**6067-6075. http://doi.org/10.1021/acsnano.0c01804

6. Lin, Z.; Yang, J.; Li, X.; Wu, Y.; Wei, W.; Liu, J.; Chen, J.; Yang, J., **Large-scale and washable smart textiles based on triboelectric nanogenerator arrays for self-powered sleeping monitoring.** Adv. Funct. Mater. 2018, **28:**1704112. http://doi.org/10.1002/adfm.201704112

7. Lai, Y. C.; Deng, J.; Zhang, S. L.; Niu, S.; Guo, H.; Wang, Z. L., **Single-thread-based wearable and highly stretchable triboelectric nanogenerators and their applications in cloth-based self-powered human-interactive and biomedical sensing.** Adv. Funct. Mater. 2017, **27:**1604462. http://doi.org/10.1002/adfm.201604462

8. Olson, K. P.; Mizzi, C. A.; Marks, L. D., **Band bending and ratcheting explain triboelectricity in a flexoelectric contact diode. Nano Lett. 2022, **22:**3914-3921. http://doi.org/10.1021/acs.nanolett.2c00107

Novel flexoelectric effect explaining triboelectricity generation in TENGs where metals and semiconductors are involved.

9. Mizzi, C. A.; Marks, L. D., **When flexoelectricity drives triboelectricity.** Nano Lett. 2022, **22:**3939–3945. http://doi.org/10.1021/acs.nanolett.2c00240

10. San, S. T.; Yun, J.; Kim, D., **Hybridized generator to simultaneously harvest tribo-thermal energy induced by vibration of fluorine rich-beads.** Nano Energy 2022, **97**. http://doi.org/10.1016/j.nanoen.2022.107211

11. Chen, J.; Wang, Z. L., **Reviving vibration energy harvesting and self-powered sensing by a triboelectric nanogenerator.** Joule 2017, **1:**480–521. http://doi.org/10.1016/j.joule.2017.09.004

12. Wang, J.; Wang, H.; Thakor, N. V.; Lee, C., **Self-powered direct muscle stimulation using a triboelectric nanogenerator (TENG) integrated with a flexible multiple-channel intramuscular electrode.** ACS Nano. 2019, **13:**3589–3599. http://doi.org/10.1021/acsnano.9b00140

13. Wang, X.; Song, J.; Liu, J.; Zhong, L. W., **Direct-current nanogenerator driven by ultrasonic waves.** Science. 2007, **316:**102–105. http://doi.org/10.1126/science.1139366

14. Tao, K.; Yi, H.; Yang, Y.; Chang, H.; Wu, J.; Tang, L.; Yang, Z.; Wang, N.; Hu, L.; Fu, Y.; Miao, J.; Yuan, W., **Origami-inspired electret-based triboelectric generator for biomechanical and ocean wave energy harvesting.** Nano Energy 2020, **67:**104197. http://doi.org/10.1016/j.nanoen.2019.104197

15. Xu, L.; Jiang, T.; Lin, P.; Shao, J. J.; He, C.; Zhong, W.; Chen, X. Y.; Wang, Z. L., **Coupled triboelectric nanogenerator networks for efficient water wave energy harvesting.** ACS Nano. 2018, **12:**1849–1858. http://doi.org/10.1021/acsnano.7b08674

16. Xi, Y.; Guo, H.; Zi, Y.; Li, X.; Wang, J.; Deng, J.; Li, S.; Hu, C.; Cao, X.; Wang, Z. L., **Multifunctional TENG for blue energy scavenging and self-powered wind-speed sensor.** Adv. Energy Mater. 2017, **7:**1602397. http://doi.org/10.1002/aenm.201602397

17. Chen, J.; Yang, J.; Li, Z.; Fan, X.; Zi, Y.; Jing, Q.; Guo, H.; Wen, Z.; Pradel, K. C.; Niu, S.; Wang, Z. L., **Networks of triboelectric nanogenerators for harvesting water wave energy: A potential approach toward blue energy.** ACS Nano. 2015, **9:**3324–3331. http://doi.org/10.1021/acsnano.5b00534

18. Zhang, S.; Bick, M.; Xiao, X.; Chen, G.; Nashalian, A.; Chen, J., **Leveraging triboelectric nanogenerators for bioengineering.** Matter 2021, **4:**845-887. http://doi.org/10.1016/j.matt.2021.01.006

19. Wang, Z. L.; Chen, J.; Niu, S.; Zi, Y.; Lin, L., **Triboelectric nanogenerators**. 1st ed. 2016: Springer International Publishing.

20. Shin, S.-H.; Kwon, Y. H.; Kim, Y.-H.; Jung, J.-Y.; Lee, M. H.; Nah, J., **Triboelectric charging sequence induced by surface functionalization as a method to fabricate high performance triboelectric generators.** ACS Nano. 2015, **9:**4621–4627. http://doi.org/10.1021/acsnano.5b01340

21. Zi, Y.; Guo, H.; Wen, Z.; Yeh, M.-H.; Hu, C.; Wang, Z. L., **Harvesting low-frequency (<5 Hz) irregular mechanical energy: a possible killer application of triboelectric nanogenerator.** ACS Nano. 2016, **10:**4797–4805. http://doi.org/10.1021/acsnano.6b01569

22. Liu, J.; Cheikh, M. I.; Bao, R.; Peng, H.; Liu, F.; Li, Z.; Jiang, K.; Chen, J.; Thundat, T., **Tribo-tunneling DC generator with carbon aerogel/silicon multi-nanocontacts.** Adv. Electron. Mater. 2019, **5:**1900464. http://doi.org/10.1002/aelm.201900464

23. Zhou, L.; Liu, D.; Wang, J.; Wang, Z. L., **Triboelectric nanogenerators: fundamental physics and potential applications.** Friction. 2020, **8:**481–506. http://doi.org/10.1007/s40544-020-0390-3

24. Akbulut, M.; Godfrey Alig, A. R.; Israelachvili, J., **Triboelectrification between smooth metal surfaces coated with self-assembled monolayers (SAMs).** J. Phys. Chem. B. 2006, **110:**22271–22278. http://doi.org/10.1021/jp063161j

25. Xu, R.; Zhang, Q.; Wang, J. Y.; Liu, D.; Wang, J.; Wang, Z. L., **Direct current triboelectric cell by sliding an n-type semiconductor on a p-type semiconductor.** Nano Energy 2019, **66:**104185. http://doi.org/10.1016/j.nanoen.2019.104185

26. Liu, L.; Zhao, Z.; Li, Y.; Li, X.; Liu, D.; Li, S.; Gao, Y.; Zhou, L.; Wang, J.; Wang, Z. L., **Achieving ultrahigh effective surface charge density of direct-current triboelectric nanogenerator in high humidity.** Small 2022, e2201402. http://doi.org/10.1002/smll.202201402

*27. Lin, S.; Lu, Y.; Feng, S.; Hao, Z.; Yan, Y., **A high current density direct-current generator based on a moving van der Waals Schottky diode.** Adv. Mater. 2018, **31:**1804398. http://doi.org/10.1002/adma.201804398

Graphene-based durable, flexible and wearable DC TENG design.

28. Lee, J. H.; Kim, S.; Kim, T. Y.; Khan, U.; Kim, S.-W., **Water droplet-driven triboelectric nanogenerator with superhydrophobic surfaces.** Nano Energy 2019, **58:**579–584. http://doi.org/10.1016/j.nanoen.2019.01.078

29. Yin, X.; Liu, D.; Zhou, L.; Li, X.; Zhang, C.; Cheng, P.; Guo, H.; Song, W.; Wang, J.; Wang, Z. L., **Structure and dimension effects on the performance of layered triboelectric nanogenerators in contact-separation mode.** ACS Nano. 2019, **13:**698–705. http://doi.org/10.1021/acsnano.8b07935

30. Liu, D.; Yin, X.; Guo, H.; Zhou, L.; Li, X.; Zhang, C.; Wang, J.; Wang, Z. L., **A constant current triboelectric nanogenerator arising from electrostatic breakdown.** Sci Adv 2019, **5:**eaav6437. http://doi.org/10.1126/sciadv.aav6437

31. Liu, W.; Wang, Z.; Wang, G.; Liu, G.; Chen, J.; Pu, X.; Xi, Y.; Wang, X.; Guo, H.; Hu, C.; Wang, Z. L., **Integrated charge excitation triboelectric nanogenerator.** Nat. Commun. 2019, **10:**1426. http://doi.org/10.1038/s41467-019-09464-8

32. Huang, X.; Xiang, X.; Nie, J.; Peng, D.; Yang, F.; Wu, Z.; Jiang, H.; Xu, Z.; Zheng, Q., **Microscale Schottky superlubric generator with high direct-current density and ultralong life. Nat. Commun. 2021, **12:**2268. http://doi.org/10.1038/s41467-021-22371-1

Description of a depletion layer estabilishment and destruction (DLED) mechanism explaining DC output from a sliding diode under minimal pressure and friction.

33. Zheng, M.; Lin, S.; Tang, Z.; Feng, Y.; Wang, Z. L., **Photovoltaic effect and tribovoltaic effect at liquid-semiconductor interface.** Nano Energy 2021, **83:**105810. http://doi.org/10.1016/j.nanoen.2021.105810

Tribovoltaic-photovoltaic coupled systems to harvest the electricity more efficiently.

34. Zheng, M.; Lin, S.; Xu, L.; Zhu, L.; Wang, Z. L., **Scanning probing of the tribovoltaic effect at the sliding interface of two semiconductors.** Adv. Mater. 2020, **32:**e2000928. http://doi.org/10.1002/adma.202000928

35. Zhang, Z.; He, T.; Zhao, J.; Liu, G.; Wang, Z. L.; Zhang, C., **Tribo-thermoelectric and tribovoltaic coupling effect at metal-semiconductor interface.** Mater. Today Phys. 2021, **16**. http://doi.org/10.1016/j.mtphys.2020.100295

36. Lin, S.; Chen, X.; Wang, Z. L., **The tribovoltaic effect and electron transfer at a liquid-semiconductor interface.** Nano Energy 2020, **76:**105070. http://doi.org/10.1016/j.nanoen.2020.105070

37. Zhang, Z.; Jiang, D.; Zhao, J.; Liu, G.; Bu, T.; Zhang, C.; Wang, Z. L., **Tribovoltaic effect on metal–semiconductor interface for direct-current low-impedance triboelectric nanogenerators.** Adv. Energy Mater. 2020, **10:**1903713. http://doi.org/10.1002/aenm.201903713

38. Zhang, J.; Coote, M. L.; Ciampi, S., **Electrostatics and electrochemistry: mechanism and scope of charge-transfer reactions on the surface of tribocharged insulators.** J. Am. Chem. Soc. 2021, **143:**3019–3032. http://doi.org/10.1021/jacs.0c11006

39. Kim, W.-G.; Kim, D.-W.; Tcho, I.-W.; Kim, J.-K.; Kim, M.-S.; Choi, Y.-K., **Triboelectric nanogenerator: Structure, mechanism, and applications.** ACS Nano. 2021, **15:**258–287. http://doi.org/10.1021/acsnano.0c09803

40. Duke, C. B.; Noolandi, J.; Thieret, T., **The surface science of xerography.** Surf. Sci. 2002, **500:**1005–1023. http://doi.org/10.1016/S0039-6028(01)01527-8

41. Wang, Z. L.; Wang, A. C., **On the origin of contact-electrification.** Mater. Today. 2019, **30:**34–51. http://doi.org/10.1016/j.mattod.2019.05.016

42. Liu, C.-y.; Bard, A. J., **Electrostatic electrochemistry: Nylon and polyethylene systems.** Chem. Phys. Lett. 2010, **485:**231–234. http://doi.org/10.1016/j.cplett.2009.12.009

43. Bard, A. J.; Liu, C., **Electrostatic electrochemistry at insulators.** Nat Mater 2008, **7:**505–509. http://doi.org/10.1038/nmat2160

44. Burgo, T. A. L.; Ducati, T. R. D.; Francisco, K. R.; Clinckspoor, K. J.; Galembeck, F.; Galembeck, S. E., **Triboelectricity: Macroscopic charge patterns formed by self-arraying ions on polymer surfaces.** Langmuir 2012, **28:**7407–7416. http://doi.org/10.1021/la301228j

45. Zhang, L.; Laborda, E.; Darwish, N.; Noble, B. B.; Tyrell, J. H.; Pluczyk, S.; Le Brun, A. P.; Wallace, G. G.; Gonzalez, J.; Coote, M. L.; Ciampi, S., **Electrochemical and electrostatic cleavage of alkoxyamines.** J. Am. Chem. Soc. 2018, **140:**766–774. http://doi.org/10.1021/jacs.7b11628

46. Zhang, J.; Rogers, F. J. M.; Darwish, N.; Gonçales, V. R.; Vogel, Y. B.; Wang, F.; Gooding, J. J.; Peiris, M. C. R.; Jia, G.; Veder, J.-P.; Coote, M. L.; Ciampi, S., **Electrochemistry on tribocharged polymers is governed by the stability of surface charges rather than charging magnitude.** J. Am. Chem. Soc. 2019, **141:**5863–5870. http://doi.org/10.1021/jacs.9b00297

47. Chaplin, M., **Theory vs Experiment: What is the surface charge of water?** Water 2009, **1:**1–28.

48. Burgo, T. A. L.; Galembeck, F.; Pollack, G. H., **Where is water in the triboelectric series?** J. Electrost. 2016, **80:**30–33. http://doi.org/10.1016/j.elstat.2016.01.002

49. Beattie, J. K.; Djerdjev, A. M., **The pristine oil/water interface: Surfactant-free hydroxide-charged emulsions.** Angew. Chem. 2004, **43:**3568–3571. http://doi.org/10.1002/anie.200453916

50. Vogel, Y. B.; Evans, C. W.; Belotti, M.; Xu, L.; Russell, I. C.; Yu, L.-J.; Fung, A. K. K.; Hill, N. S.; Darwish, N.; Gonçales, V. R.; Coote, M. L.; Swaminathan Iyer, K.; Ciampi, S., **The corona of a surface bubble promotes electrochemical reactions.** Nat. Commun. 2020, **11:**6323-6323. http://doi.org/10.1038/s41467-020-20186-0

51. Ciampi, S.; Iyer, K. S., **Bubbles pinned on electrodes: Friends or foes of aqueous electrochemistry?** Curr. Opin. Electrochem. 2022, **34**. http://doi.org/10.1016/j.coelec.2022.100992

52. Lin, S.; Xu, L.; Chi Wang, A.; Wang, Z. L., **Quantifying electron-transfer in liquid-solid contact electrification and the formation of electric double-layer.** Nat. Commun. 2020, **11:**399. http://doi.org/10.1038/s41467-019-14278-9

53. Chen, Z.; Khajeh, A.; Martini, A.; Kim, S. H., **Chemical and physical origins of friction on surfaces with atomic steps.** Sci Adv 2019, **5:**eaaw0513. http://doi.org/10.1126/sciadv.aaw0513

54. McCarty, L. S.; Whitesides, G. M., **Electrostatic charging due to separation of ions at interfaces: contact electrification of ionic electrets.** Angew. Chem. 2008, **47:**2188–2207. http://doi.org/10.1002/anie.200701812

55. Gooding, D. M.; Kaufman, G. K., **Tribocharging and the triboelectric series**. Chichester, UK: John Wiley & Sons, Ltd: Chichester, UK, (2011); pp 1–14.http://doi.org/10.1002/9781119951438.eibc2239.pub2

56. Zhang, J.; Ciampi, S., **Shape and charge: Faraday's ice pail experiment revisited.** ACS Cent. Sci 2020, **6:**611–612. http://doi.org/10.1021/acscentsci.0c00298

57. Zhang, J.; Darwish, N.; Coote, M. L.; Ciampi, S., **Static electrification of plastics under friction: The position of engineering-grade polyethylene terephthalate in the triboelectric series.** Adv. Eng. Mater. 2019.

58. Zhang, J.; Ferrie, S.; Zhang, S.; Vogel, Y. B.; Peiris, C. R.; Darwish, N.; Ciampi, S., **Single-electrode electrochemistry: chemically engineering surface adhesion and hardness to maximize redox work extracted from tribocharged silicon.** ACS Appl. Nano Mater. 2019, **2:**7230–7236. http://doi.org/10.1021/acsanm.9b01726

59. Zhang, J.; Su, C.; Rogers, F. J. M.; Darwish, N.; Coote, M. L.; Ciampi, S., **Irreproducibility in the triboelectric charging of insulators: Evidence of a non-monotonic charge: Versus contact time relationship.** Phys. Chem. Chem. Phys. 2020, **22:**11671–11677. http://doi.org/10.1039/d0cp01317j

60. Jacobs, H. O.; Campbell, S. A.; Steward, M. G., **Approaching nanoxerography: The use of electrostatic forces to position nanoparticles with 100 nm scale resolution.** Adv. Mater 2002, **14:**1553-1557. http://doi.org/10.1002/1521-4095(20021104)14:21<1553::AID-ADMA1553>3.0.CO;2-9

61. Palleau, E.; Sangeetha, N. M.; Viau, G.; Marty, J.-D.; Ressier, L., **Coulomb force directed single and binary assembly of nanoparticles from aqueous dispersions by AFM nanoxerography.** ACS Nano. 2011, **5:**4228–4235. http://doi.org/10.1021/nn2011893

62. Liu, J.; Goswami, A.; Jiang, K. R.; Khan, F.; Kim, S.; McGee, R.; Li, Z.; Hu, Z. Y.; Lee, J.; Thundat, T., **Direct-current triboelectricity generation by a sliding Schottky

nanocontact on MoS_2 multilayers. Nat. Nanotechnol. 2018, **13:**112–116. http://doi.org/10.1038/s41565-017-0019-5

First demonstration of continuous DC output from an out-of-equilibrium sliding Schottky nanocontact without an external voltage.

63. Shao, H.; Fang, J.; Wang, H.; Dai, L.; Lin, T., **Polymer-metal Schottky contact with direct-current outputs.** Adv. Mater 2016, **28:**1461–1466. http://doi.org/10.1002/adma.201504778

64. Linford, M. R.; Chidsey, C. E. D., **Alkyl monolayers covalently bonded to silicon surfaces.** J. Am. Chem. Soc. 1993, **115:**12631-12632. http://doi.org/10.1021/ja00079a071

65. Hunger, R.; Jaegermann, W.; Merson, A.; Shapira, Y.; Pettenkofer, C.; Rappich, J., **Electronic Structure of Methoxy-, Bromo-, and Nitrobenzene Grafted onto Si(111).** J. Phys. Chem. B 2006, **110:**15432-15441. http://doi.org/10.1021/jp055702v

66. Barrelet, C. J.; Robinson, D. B.; Cheng, J.; Hunt, T. P.; Quate, C. F.; Chidsey, C. E. D., **Surface characterization and electrochemical properties of alkyl, fluorinated alkyl, and alkoxy monolayers on silicon.** Langmuir 2001, **17:**3460–3465. http://doi.org/10.1021/la010333p

67. Kim, I.; Roh, H.; Yu, J.; Jeon, H.; Kim, D., **A triboelectric nanogenerator using silica-based powder for appropriate technology.** Sens. Actuators, A 2018, **280:**85–91. http://doi.org/10.1016/j.sna.2018.07.013

68. Lyu, X.; Ferrie, S.; Pivrikas, A.; MacGregor, M.; Ciampi, S., **Sliding Schottky diode triboelectric nanogenerators with current output of 10^9A/m^2 by molecular engineering of Si(211) surfaces. Nano Energy 2022, 107658. http://doi.org/https://doi.org/10.1016/j.nanoen.2022.107658

Altering surface recombination velocity by means of surface chemistry as a way to maximize DC outputs. Modification of Si(211) with proton-exchangeable organic monolayers enhances DC outputs.

69. Yang, R.; Xu, R.; Dou, W.; Benner, M.; Zhang, Q.; Liu, J., **Semiconductor-based dynamic heterojunctions as an emerging strategy for high direct-current mechanical energy harvesting.** Nano Energy 2021, **83:**105849. http://doi.org/10.1016/j.nanoen.2021.105849

70. Chaudhury, M. K., **Adhesion and friction of self-assembled organic monolayers.** Curr. Opin. Colloid Interface Sci. 1997, **2:**65–69. http://doi.org/10.1016/S1359-0294(97)80009-X

71. Kim, H. I.; Koini, T.; Lee, T. R.; Perry, S. S., **Systematic studies of the frictional properties of fluorinated monolayers with atomic force microscopy: Comparison of CF_3- and CH_3-terminated films.** Langmuir 1997, **13:**7192–7196. http://doi.org/10.1021/la970539j

72. Ehlert, G. J.; Galan, U.; Sodano, H. A., **Role of surface chemistry in adhesion between ZnO nanowires and carbon fibers in hybrid composites.** ACS Appl. Mater. Interfaces. 2013, **5:**635–645. http://doi.org/10.1021/am302060v

*73. Ferrie, S.; Le Brun, A. P.; Krishnan, G.; Andersson, G. G.; Darwish, N.; Ciampi, S., **Sliding silicon-based Schottky diodes: Maximizing triboelectricity with surface chemistry.** Nano Energy 2022, **93:**106861. http://doi.org/10.1016/j.nanoen.2021.106861

DC from a sliding Schottky diode doubled by silicon surface chemistry engineering. Sliding platinum contacts output greater current and lead to larger excess friction on n-Si than on p-Si.

*74. Liu, J.; Zhang, Y.; Chen, J.; Bao, R.; Jiang, K.; Khan, F.; Goswami, A.; Li, Z.; Liu, F.; Feng, K.; Luo, J.; Thundat, T., **Separation and quantum tunneling of photo-generated carriers using a tribo-induced field.** Matter 2019, **1:**650–660. http://doi.org/10.1016/j.matt.2019.05.017

Photocurrent strongly amplified by friction-induced voltages.

75. Liu, J.; Miao, M.; Jiang, K.; Khan, F.; Goswami, A.; McGee, R.; Li, Z.; Nguyen, L.; Hu, Z.; Lee, J.; Cadien, K.; Thundat, T., **Sustained electron tunneling at unbiased metal-insulator-semiconductor triboelectric contacts.** Nano Energy 2018, **48:**320-326. http://doi.org/https://doi.org/10.1016/j.nanoen.2018.03.068

76. Vogel, Y. B.; Zhang, L.; Darwish, N.; Gonçales, V. R.; Le Brun, A.; Gooding, J. J.; Molina, A.; Wallace, G. G.; Coote, M. L.; Gonzalez, J.; Ciampi, S., **Reproducible flaws unveil electrostatic aspects of semiconductor electrochemistry.** Nat. Commun. 2017, **8:**2066. http://doi.org/10.1038/s41467-017-02091-1

77. Aragonès, A. C.; Darwish, N.; Ciampi, S.; Sanz, F.; Gooding, J. J.; Diéz-Pérez, I., **Single-molecule electrical contacts on silicon electrodes under ambient conditions.** Nat. Commun. 2017, **8:**15056. http://doi.org/10.1038/ncomms15056

78. Peiris, C. R.; Ferrie, S.; Ciampi, S.; Rickard, W. D. A.; Darwish, N., **Memristor arrays formed by reversible formation and breakdown of nanoscale silica layers on Si–H surfaces.** ACS Appl. Nano Mater. 2022, **5:**6609–6617. http://doi.org/10.1021/acsanm.2c00663

79. Li, T.; Dief, E. M.; Lyu, X.; Rahpeima, S.; Ciampi, S.; Darwish, N., **Nanoscale silicon oxide reduces electron transfer kinetics of surface-bound ferrocene monolayers on dilicon.** J. Phys. Chem. C. 2021, **125:**27763–27770. http://doi.org/10.1021/acs.jpcc.1c07788

80. Zhang, S.; Ferrie, S.; Lyu, X.; Xia, Y.; Darwish, N.; Wang, Z.; Ciampi, S., **Absence of a relationship between surface conductivity and electrochemical rates: redox-active monolayers on Si(211), Si(111), and Si(110).** J. Phys. Chem. C 2021, **125:**18197–18203. http://doi.org/10.1021/acs.jpcc.1c05023

81. Dief, E. M.; Brun, A. P. L.; Ciampi, S.; Darwish, N., **Spontaneous grafting of OH-terminated molecules on Si−H surfaces via Si–O–C covalent bonding.** Surfaces 2021, **4:**81–88. http://doi.org/10.3390/surfaces4010010

82. Veerbeek, J.; Huskens, J., **Applications of monolayer-functionalized H-terminated silicon surfaces: A review.** Small Methods 2017, **1:**1700072. http://doi.org/10.1002/smtd.201700072

83. Linford, M. R.; Fenter, P.; Eisenberger, P. M.; Chidsey, C. E. D., **Alkyl monolayers on silicon prepared from 1-alkenes and hydrogen-terminated silicon.** J. Am. Chem. Soc. 1995, **117:**3145–3155. http://doi.org/10.1021/ja00116a019

84. Ferrie, S.; Darwish, N.; Gooding, J. J.; Ciampi, S., **Harnessing silicon facet-dependent conductivity to enhance the direct-current produced by a sliding Schottky diode triboelectric nanogenerator. Nano Energy 2020, **78:**105210. http://doi.org/10.1016/j.nanoen.2020.105210

Schottky diode DC TENG output maximized at concave rather than at convex boundaries between different silicon crystallographic planes.

85. Zhao, Y.; Descamps, J.; Ababou-Girard, S.; Bergamini, J. F.; Santinacci, L.; Léger, Y.; Sojic, N.; Loget, G., **Metal-insulator-semiconductor anodes for ultrastable and site-selective upconversion photoinduced electrochemiluminescence.** Angew. Chem. 2022, **134:**n/a. http://doi.org/10.1002/ange.202201865

86. Loget, G.; Fabre, B.; Fryars, S. p.; Mériadec, C.; Ababou-Girard, S., **Dispersed Ni nanoparticles stabilize silicon photoanodes for efficient and inexpensive sunlight-assisted water oxidation.** ACS Energy Lett. 2017, **2:**569–573. http://doi.org/10.1021/acsenergylett.7b00034

87. Zhao, Y.; Yu, J.; Xu, G.; Sojic, N.; Loget, G., **Photoinduced electrochemiluminescence at silicon electrodes in water.** J. Am. Chem. Soc. 2019, **141:**13013–13016. http://doi.org/10.1021/jacs.9b06743

88. Wagle, D. V.; Baker, G. A., **Cold welding: a phenomenon for spontaneous self-healing and shape genesis at the nanoscale.** Mater. Horiz. 2015, **2:**157-167. http://doi.org/10.1039/c4mh00105b

*89. Wang, S.; Zi, Y.; Zhou, Y. S.; Li, S.; Fan, F.; Lin, L.; Wang, Z. L., **Molecular surface functionalization to enhance the power output of triboelectric nanogenerators.** J. Mater. Chem. A. 2016, **4:**3728–3734. http://doi.org/10.1039/c5ta10239a

Self-assembled monolayers (SAMs) influence on TENGs output.

90. You, Z.; Wang, S.; Li, Z.; Zou, Y.; Lu, T.; Wang, F.; Hu, B.; Wang, X.; Li, L.; Fang, W.; Liu, Y., **High current output direct-current triboelectric nanogenerator based on organic semiconductor heterojunction.** Nano Energy 2022, **91:**106667. http://doi.org/10.1016/j.nanoen.2021.106667

91. Xu, C.; Liu, Y.; Liu, Y.; Zheng, Y.; Feng, Y.; Wang, B.; Kong, X.; Zhang, X.; Wang, D., **New inorganic coating-based triboelectric nanogenerators with anti-wear and self-healing properties for efficient wave energy harvesting.** Appl. Mater. Today 2020, **20:**100645. http://doi.org/10.1016/j.apmt.2020.100645

92. Zeng, Q.; Wu, Y.; Tang, Q.; Liu, W.; Wu, J.; Zhang, Y.; Yin, G.; Yang, H.; Yuan, S.; Tan, D.; Hu, C.; Wang, X., **A high-efficient breeze energy harvester utilizing a full-packaged triboelectric nanogenerator based on flow-induced vibration.** Nano Energy 2020, **70:**104524. http://doi.org/10.1016/j.nanoen.2020.104524

93. Chen, P.; An, J.; Shu, S.; Cheng, R.; Nie, J.; Jiang, T.; Wang, Z. L., **Super-durable, low-wear, and high-performance fur-brush triboelectric nanogenerator for wind and water energy harvesting for smart agriculture.** Adv. Energy Mater. 2021, **11:**2003066. http://doi.org/10.1002/aenm.202003066

*94. Chen, S.; Liu, D.; Zhou, L.; Li, S.; Zhao, Z.; Cui, S.; Gao, Y.; Li, Y.; Wang, Z. L.; Wang, J., **Improved output performance of direct-current triboelectric nanogenerator through field enhancing breakdown effect.** Adv. Mater. Technol. 2021, **6:**2100195. http://doi.org/10.1002/admt.202100195

DC TENGs improved performances via breakdown using a structure containing a triboelectric layer and a pre-charged electret layer.

95. Berman, D.; Erdemir, A.; Sumant, A. V., **Graphene: a new emerging lubricant.** Mater. Today. 2014, **17:**31–42. http://doi.org/10.1016/j.mattod.2013.12.003

96. Ciampi, S.; Eggers, P. K.; Le Saux, G.; James, M.; Harper, J. B.; Gooding, J. J., **Silicon (100) Electrodes Resistant to Oxidation in Aqueous Solutions: An Unexpected Benefit of Surface Acetylene Moieties.** Langmuir 2009, **25:**2530-2539. http://doi.org/10.1021/la803710d

97. Peiris, C. R.; Ferrie, S.; Ciampi, S.; Rickard, W. D. A.; Darwish, N., **Memristor arrays formed by reversible formation and breakdown of nanoscale silica layers on Si–H surfaces.** ACS Appl. Nano Mater. 2022, **5:**6609–6617. http://doi.org/10.1021/acsanm.2c00663

98. Abadal, G.; Pérez-Murano, F.; Barniol, N.; Aymerich, X., **Field induced oxidation of silicon by SPM: study of the mechanism at negative sample voltage by STM, ESTM and AFM.** Appl. Phys. A: Mater. Sci. Process. 1998, **66:**S791–S795. http://doi.org/10.1007/s003390051244

99. Lu, Y.; Feng, S.; Shen, R.; Xu, Y.; Hao, Z.; Yan, Y.; Zheng, H.; Yu, X.; Gao, Q.; Zhang, P.; Lin, S., **Tunable dynamic black phosphorus/insulator/Si heterojunction direct-current generator based on the hot electron transport.** Research 2019, **2019:**5832382. http://doi.org/10.34133/2019/5832382

100. Pang, J.; Bachmatiuk, A.; Yin, Y.; Trzebicka, B.; Zhao, L.; Fu, L.; Mendes, R. G.; Gemming, T.; Liu, Z.; Rummeli, M. H., **Applications of phosphorene and black phosphorus in energy conversion and storage devices.** Adv. Energy Mater. 2018, **8:**1702093. http://doi.org/10.1002/aenm.201702093

101. Lu, Y.; Gao, Q.; Yu, X.; Zheng, H.; Shen, R.; Hao, Z.; Yan, Y.; Zhang, P.; Wen, Y.; Yang, G.; Lin, S., **Interfacial built-in electric field-driven direct current generator based on dynamic silicon homojunction.** Research 2020, **2020:**5714754. http://doi.org/10.34133/2020/5714754

*102. Liu, J.; Liu, F.; Bao, R.; Jiang, K.; Khan, F.; Li, Z.; Peng, H.; Chen, J.; Alodhayb, A.; Thundat, T., **Scaled-up direct-current generation in MoS_2 multilayer-based moving heterojunctions.** ACS Appl. Mater. Interfaces. 2019, **11:**35404–35409. http://doi.org/10.1021/acsami.9b09851

Seminal study of the influence of the dielectric material and its thickness on the output of DC TENGs.

103. Lu, Y.; Yan, Y.; Yu, X.; Zhou, X.; Feng, S.; Xu, C.; Zheng, H.; Yang, Z.; Li, L.; Liu, K.; Lin, S., **Polarized water driven dynamic PN junction-based direct-current generator. Research 2021, **2021:**7505638. http://doi.org/10.34133/2021/7505638

Water flowing between two semiconductors outputs 0.3 V and a DC of 0.6 μA.

*104. Sharov, V. A.; Alekseev, P. A.; Borodin, B. R.; Dunaevskiy, M. S.; Reznik, R. R.; Cirlin, G. E., **InP/Si heterostructure for high-current hybrid triboelectric/photovoltaic generation.** ACS Appl. Energy Mater. 2019, **2:**4395–4401. http://doi.org/10.1021/acsaem.9b00576

Demonstration that dark current originates from the tunneling and is separate from photoeffects.